ChemSusChem

Research Article
doi.org/10.1002/cssc.202201329

Chemistry Europe
European Chemical Societies Publishing

www.chemsuschem.org

Bicarbonate Electroreduction to Multicarbon Products Enabled by Cu/Ag Bilayer Electrodes and Tailored Microenviroments

Jungkuk Lee,[a] Hengzhou Liu,[a] and Wenzhen Li*[a]

Bicarbonate electrolyzer can achieve the direct conversion of CO_2 capture solutions that bypasses energy-intensive steps of CO_2 regeneration and pressurization. However, only single-carbon chemicals (i.e., CO, formate, CH_4) were reported as the major products so far. Herein, bicarbonate conversion to multicarbon (C_{2+}) products (i.e., acetate, ethylene, ethanol, propanol) was achieved on rationally designed Cu/Ag bilayer electrodes with bilayer cation- and anion-conducting ionomers. The in-situ generated CO_2 was first reduced to CO on the Ag layer, followed by its favorable further reduction to C_{2+} products on the Cu layer, benefiting from the locally high concentration of CO. Through optimizing the bilayer configurations, metal compositions, ionomer types, and local hydrophobicity, a microenvironment was created (high local pH, low water content, etc.) to enhance bicarbonate-to-C_{2+} conversion and suppress the hydrogen evolution reaction. Subsequently, a maximum C_{2+} faradaic efficiency of $41.6 \pm 0.39\%$ was achieved at a considerable current density of 100 mA cm^{-2}.

Introduction

Electrochemical CO_2 reduction (eCO_2R) to value-added chemicals and fuels has been intensively studied as a potential technology to address the challenges in reducing greenhouse gas emissions (GHG).[1] Most CO_2 electrolyzers were supplied with pressurized high-purity CO_2.[2] However, the utilization of purified CO_2 requires multiple energy-intensive steps, including capturing CO_2 from diluted sources (e.g., from the air), and regeneration and pressurization of CO_2 from the capture media, which largely increase the production costs and lower the overall energy efficiency.[3] Besides, most conventional purified CO_2-fed electrolyzers showed low carbon utilization (especially in the alkaline flow electrolyzers); consequently, more energy is consumed to provide excessive CO_2.[4]

Alternatively, direct electrochemical conversion of CO_2 capture solutions (instead of gaseous CO_2) into valuable chemicals can circumvent the energy-intensive CO_2 regeneration and pressurization steps.[5] In bipolar membrane (BPM)-based electrolyzers, aqueous bicarbonate (HCO_3^-) can react with H^+, which is directly supplied from the BPM through water dissociation, to form in situ CO_2 [*i*-CO_2, Eq. (1)].[6] Then, the *i*-CO_2 can be electrochemically reduced into valuable carbon products (Figure 1).

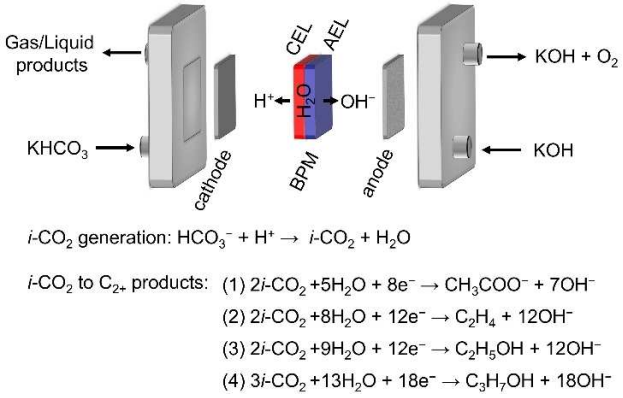

Figure 1. Schematic diagram of bicarbonate electrolyzer and reaction chemistry to C_{2+} products. A bipolar membrane dissociates H_2O and supplies H^+ to the cathode side resulting in in-situ generation of CO_2 (*i*-CO_2), which is further reduced on the cathode. AEL: anion exchange layer, CEL: cation exchange layer.

$$HCO_3^-{}_{(aq)} + H^+{}_{(aq)} \rightarrow CO_{2(g)} + H_2O_{(l)} \quad (1)$$

For instance, Berlinguette and co-workers reported faradaic efficiency (FE) of >60% toward CO and formate at the current densities of >100 mA cm^{-2},[7] and the FE of 34% toward CH_4 at a partial current density of 120 mA cm^{-2}.[8] Despite significant research progress in C_1 product generation, multicarbon (C_{2+}) (i.e., acetate, ethylene, ethanol, propanol) as the major products were rarely reported in the bicarbonate-based system.

The C_{2+} products are considered more promising than the C_1 products in terms of market size and value. Copper (Cu) is the only unique metal to produce C_{2+} products.[9] In the gaseous CO_2-fed electrolyzers, enormous efforts have been paid to improve C_{2+} FE by designing Cu-based monometallic or bimetallic catalysts and modifying their local environments.[10] For instance, tandem catalysts (e.g., Cu/Ag, Cu/Fe–N–C)

[a] Dr. J. Lee, Dr. H. Liu, Prof. Dr. W. Li
Department of Chemical and Biological Engineering
Iowa State University
50011 Ames, IA (US)
E-mail: wzli@iastate.edu

Supporting information for this article is available on the WWW under https://doi.org/10.1002/cssc.202201329

exhibited an increase in C_{2+} FE, which benefited from a high *CO coverage (key intermediate for C–C coupling) due to the incorporation of the second metal other than Cu.[10d] However, limited research efforts were devoted to the direct conversion of bicarbonate toward C_{2+} products in the BPM-based electrolyzer, and their FE remain very low (< 15% on the monometallic Cu electrode).[11] The bicarbonate-to-C_{2+} conversion is more challenging than direct CO_2 electrolyzers fed with gaseous CO_2, mainly due to the inadequate local *i*-CO_2 concentration (or low *CO coverage). In addition, the near-neutral pH (i.e., bicarbonate buffered electrolyte) is another major obstacle to C_{2+} production. The C–C coupling in its formation of C_{2+} products is more favorable in an alkaline environment, while lowering the electrolyte pH to near neutral would favor the hydrogen evolution reaction (HER).[12] These challenges motivate us to design bilayer electrodes and optimize their microenvironments for increasing local *CO coverage, facilitating C–C coupling, and suppressing HER.

Here, we present the rationally designed Cu/Ag bilayer electrodes with bi-ionomers to maximize the bicarbonate-to-C_{2+} conversion. The Ag layer with Nafion ionomer facilitates *i*-CO_2 reduction to CO intermediate, then the Cu layer with a Sustanion ionomer efficiently converts CO to C_{2+} products by maintaining high local pH (through OH^- trapping).[10e,13] The local environments were modified by using a hydrophobic substrate and adding polytetrafluoroethylene (PTFE) nanopowder in the Ag layer, which can significantly enhance the transport of gaseous reactant (*i*-CO_2) and intermediate (CO), and simultaneously suppress the HER. As such, the rationally designed bilayer cathode with Cu and Ag catalysts showed maximum C_{2+} FE of 41.6 ± 0.39% at a current density of 100 mA cm^{-2}.

Results and Discussion

We first evaluated the bicarbonate-to-C_{2+} performance on commercial Cu nanoparticles, which were mixed with a Nafion ionomer (CuNaf) and spray-coated on a hydrophilic carbon paper (H23). The electrolysis was performed in a zero-gap membrane electrode assembly (MEA)-based flow electrolyzer, with aqueous $KCHO_3$ and KOH fed as the catholyte and anolyte, respectively (Figure 1). Figure 2a and Figure S1 show that HER was the dominant reaction with an H_2 FE of 75%. C_{2+} products were indeed observed but with significantly low FE: 2.9% of ethylene, 3.6% of ethanol, and no detectable acetate and propanol. Obviously, these low FEs are due to the low surface coverage of adsorbed carbon monoxide (*CO), which is the critical intermediate to C_{2+} products on Cu-based electrodes,[14] and the near-neutral pH in the bicarbonate buffered system, which is a key factor that suppressed C–C coupling.[12a,c]

To improve the surface coverage of *CO, we implemented a bimetallic configuration through mixing commercial Ag and Cu nanoparticles with Nafion ionomer (CuAgNaf). This bimetallic system can facilitate *i*-CO_2-to-CO conversion on the Ag sites, and further reduce CO-to-C_{2+} products on the adjacent Cu sites. As shown in Figure S2, although the CuAgNaf catalyst showed an increase of CO FE (7%) compared to the CuNaf (4.5%), the

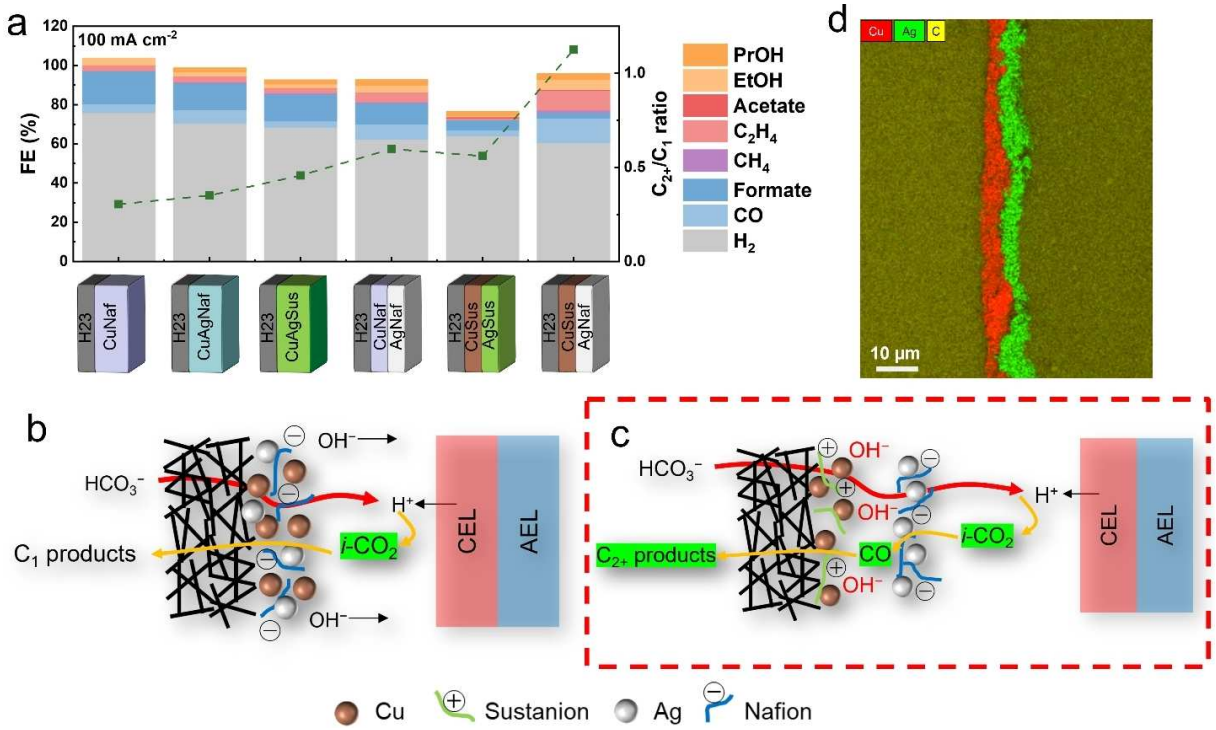

Figure 2. (a) FE and C_{2+}/C_1 ratio over six different configurations of catalyst and ionomer layers. The bicarbonate conversion was performed at a current density of 100 mA cm^{-2} for 1 h. Schematic illustration of microstructure of (b) CuAgNaf and (c) CuSus/AgNaf. (d) Cross-sectional EDS mapping of the CuSus/AgNaf bilayer electrode prepared by epoxy embedding (see the Supporting Information for details).

C_{2+} FE remained low (7.4%), indicating other factors (e.g., local pH) may limit the C_{2+} formation.[12a,c] However, in the bicarbonate buffered system, it is difficult to adjust pH to high alkalinity because of the conversion of HCO_3^- to CO_3^{2-}. Besides, the use of a single Nafion ionomer as the catalyst binder and ion conductor (Figure 2b), which contains negative charges on their functional groups to conduct cations, would expel hydroxide ions (OH^-) from the catalyst surface and make it impossible to create a high local pH.

Inspired by a previous purified CO_2-fed system using bi-ionomer layers on the copper electrode,[10e] we further rationally designed a bilayer configuration with two kinds of catalysts and two types of ionomers for direct electroreduction of bicarbonate (Figure 2c). The first layer on the carbon paper substrate is a Cu layer with Sustanion ionomer (CuSus), which is a positively charged anion-conducting ionomer that can attract OH^- to the electrode surface. The second layer, on the top of CuSus, is an Ag layer with Nafion ionomer (AgNaf). This Nafion ionomer will transport H^+ from the BPM for its subsequent formation of *i*-CO_2,[7b] which will be instantly reduced to CO on the Ag surface. Subsequently, CO can penetrate the AgNaf layer and be further reduced to C_{2+} on the CuSus layer under an alkaline environment induced by OH^- trapping. This bilayer configuration with bi-ionomer (CuSus/AgNaf) was compared with bilayer with single ionomer (CuNaf/AgNaf, CuSus/AgSus) to verify the necessity of bi-ionomer structure. Scanning electron microscopy (SEM) images and energy-dispersive X-ray spectroscopy (EDS) mapping of CuSus/AgNaf showed a well-defined bilayer structure (Figure 2d, Figure S3). At the current density of 100 mA cm^{-2}, the CuSus/AgNaf electrode indeed exhibited a great increase in C_{2+} performance (FE of 18.6%), which significantly outperformed that of CuNaf (6.5%), CuAgNaf (7.4%), and CuNaf/AgNaf (11.4%), and CuSus/AgSus (4.6%), (Figure 2a and Figure S4). In addition to the FE, CuSus/AgNaf showed higher *i*-CO_2 generation (1.9 mM) and *i*-CO_2 utilization (3.7%) to C_{2+} products compared to the that of CuNaf/AgNaf (1.6 mM, 2.8%) and CuSus/AgSus (1.2 mM, 0.2%), indicating applying bi-ionomer structure is critical to *i*-CO_2 formation and utilization (Figure S5). The FE ratio of C_{2+} to C_1 products was greatly increased from 0.3 (CuNaf) to 1.1% (CuSuS/AgNaf) with concurrent suppression of H_2 from 75.8 to 60.6%. The optimal loading of Sustanion ionomer in CuSus/AgNaf was found to be 20 wt% (Figure S6). It is worth noting that the cell voltages are stabilized between 3.6–3.7 V on all tested electrodes (Figure S7), suggesting the unaffected electrode conductivity by using different catalyst layers and ionomers.

The above electrode with bimetals and bi-ionomers (CuSus/AgNaf) not only increased the local CO concentration through the incorporation of the Ag layer, but also created a favorable local pH by OH^- trapping into the CuSus layer. However, HER was still a dominant reaction (H_2 FE: 60.6%), which could be due to the low hydrophobicity of catalyst layers and carbon paper substrate (namely H23). Although the direct feeding of aqueous bicarbonate into the electrolyzer, the gaseous *i*-CO_2 is the actual reactant for eCO_2R in the BPM-based electrolytic system. As such, in addition to the local high pH, it is important to further create a hydrophobic microenvironment that can facilitate the transport of *i*-CO_2 and CO intermediates through the gas diffusion layer (GDL), resulting in an increase in their concentration and utilization. Meanwhile, the HER can be further suppressed under this environment with low water content.

Driven by those hypotheses, we further modified the carbon-based substrate and incorporated hydrophobic additives to further optimize the microenvironment. When we implemented a commercial hydrophobic carbon paper (namely 22BB), which has a microporous layer (MPL) with 5% of PTFE, to substitute H23 (an untreated plain carbon paper), the C_{2+} FE was improved from 18.6 to 26.0% along with slightly suppressed HER (H_2 FE: 57%) (Figure S8). Furthermore, after 50 wt% of PTFE nanopowder was incorporated into the catalyst layers, specifically in the Ag layer (CuSus/AgNaf-P), the H_2 FE was greatly minimized to only 33%, with maximum C_{2+} FE of 41.6% (Figure 3a). Contact angle measurement suggested a

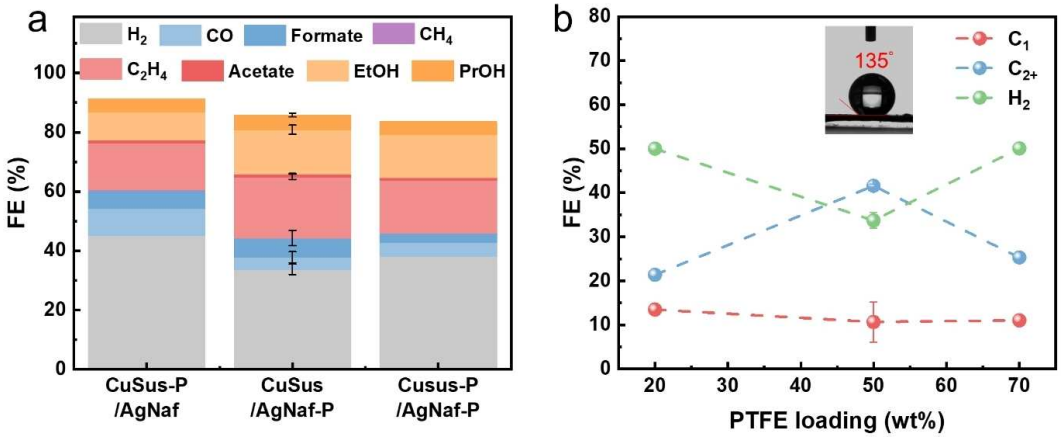

Figure 3. Dependency of hydrophobicity on bicarbonate conversion to C_{2+} products. (a) Comparison of FE after addition of PTFE in different catalyst layers on 22BB carbon paper substrate. (b) FE of C_1, C_{2+}, and H_2 as a function of PTFE loading on CuSus/AgNaf-P. The PTFE loading was varied only on the Ag layer. The electrolysis was performed at the constant current density of 100 mA cm^{-2} for 1 h. Inset image: contact angle measurement of CuSus/AgNaf-P50. The contact angle was measured in five different regions and the average value was reported.

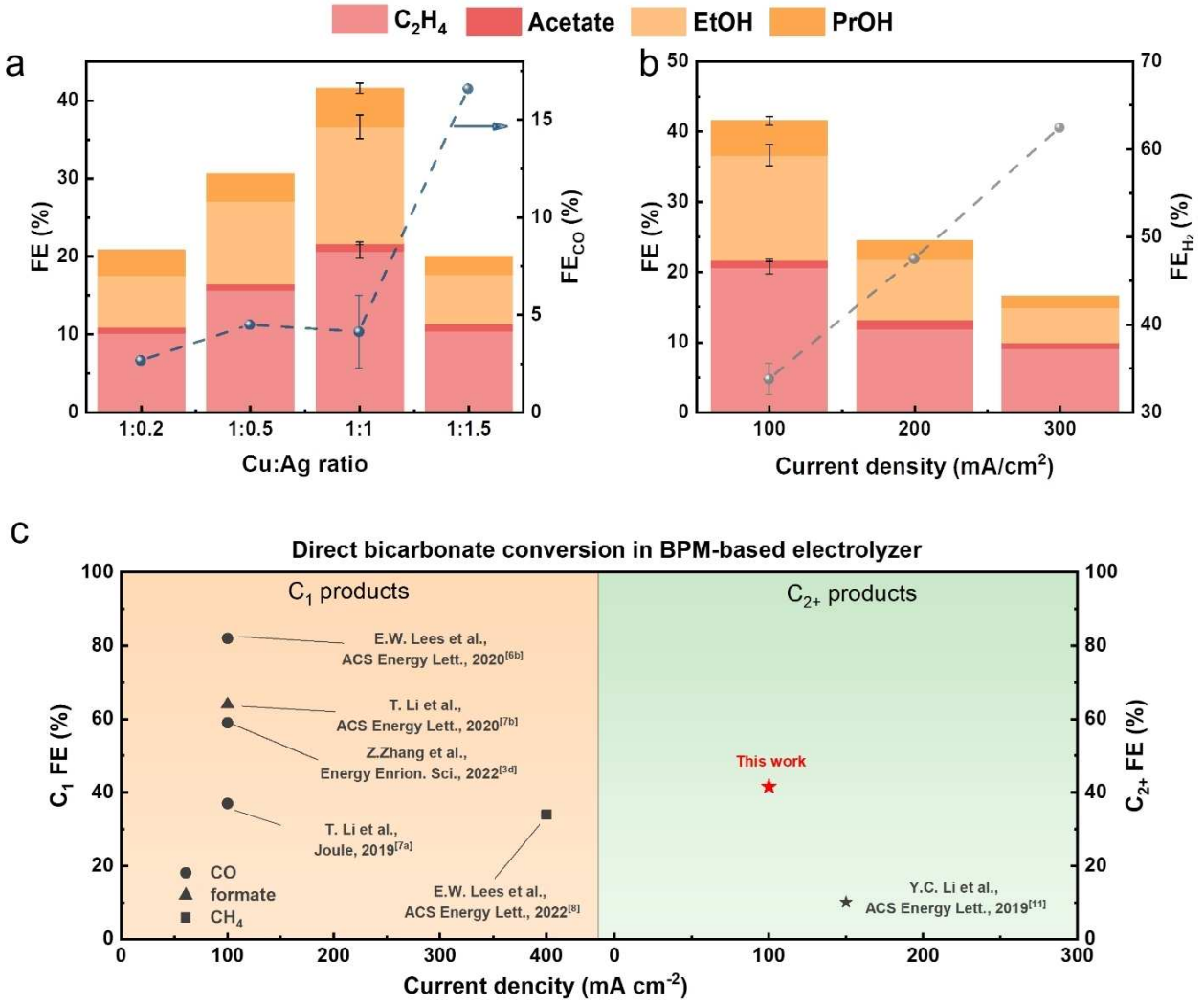

Figure 4. FE of products on CuSus/AgNaf-P50 as a function of (a) Cu/Ag ratio at a current density of 100 mA cm^{-2}, and (b) current densities from 100 to 300 mA cm^{-2}. The catholyte for 100 and 150 mA cm^{-2} was 40 mL of 3 M $KHCO_3$, while its volume was increased to 120 mL for the current density in the range of 200–300 mA cm^{-2}. (c) Comparison of eCO_2R performance of state-of-the-art coupled CO_2 capture and reduction systems.

superhydrophobic surface with a contact angle of 135° (Figure 3b). This strong hydrophobicity can be maintained after 1 h electrolysis (slightly decrease of contact angle to 108°) (Figure S9). It is worth noting that the incorporation of PTFE into the Ag layer (CuSus/AgNaf-P) is more effective than its incorporation into the Cu layer (CuSus-P/AgNaf) or both layers (CuSus-P/AgNaf-P) in the suppression of H_2 (Figure 3a). This can be rationalized because HER is more likely to dominate at the Ag layer: the favorable H^+ trapping (from H_2O dissociation in BPM) through the negatively charged Nafion ionomer could occur in this layer, which favors HER at the AgNaf/BPM interface.

Additional experiments were performed to optimize the PTFE content and the Cu/Ag ratios in order to better manage the local environments. We observed that optimized PTFE content of 50 wt% (Figure 3b) can significantly suppress HER, and the Cu/Ag ratio of 1:1 (Figure 4a) can finely tune the relative rates between *i*-CO_2-to-CO conversion on AgNaf layer and the CO-to-C_{2+} conversion on CuSus layer. Moreover, we observed that the current density of 100 mA cm^{-2} is the optimal condition with C_{2+} FE of 41.6%. Further increase in current densities led to an elevated H_2 production rate, mainly due to the insufficient *i*-CO_2 generated from HCO_3^- (Figure 4b). The design of advanced catalysts to further increase C_{2+} FEs is worth devoting more effort to in future studies, particularly in the bicarbonate reduction system with high current densities.

Conclusion

We have demonstrated bicarbonate conversion to C_{2+} products by rational design of bilayer electrodes and tailoring their microenvironments. The system with bimetals and bi-ionomers (i.e., CuSus/AgNaf) showed a promising bicarbonate-to-C_{2+} rate, benefiting from the high *CO coverage and local alkaline environment. Through the incorporation of polytetrafluoro-

ethylene into the Ag layer and the utilization of hydrophobic carbon paper, we can further create a hydrophobic environment to facilitate the transport of reactant *i*-CO_2 and intermediate CO and simultaneously suppress the hydrogen evolution reaction. After detailed system optimizations, we have achieved the maximum C_{2+} faradaic efficiency (FE) of 41.6 ± 0.39% at a considerable current density of 100 mA cm^{-2}. To the best of our knowledge, this FE is the highest reported value for direct conversion of HCO_3^- toward C_{2+} products in the bipolar membrane-based system (Figure 4c, Table S1). In addition to the most reported bicarbonate conversion to C_1 products (CO, formate, and CH_4), this work offered strategies to couple CO_2 capture and electrochemical CO_2 reduction for one-step direct production of C_{2+} chemicals and fuels with higher market size and values.

Experimental Section

Preparation of electrodes

The electrodes in this study were prepared by the spray-coating of catalysts on the different type of carbon papers. Specifically, CuNaf catalyst was prepared by mixing of 30 mg of commercial Cu nanoparticles (Sigma Aldrich, 25 nm), 180 μL of 5% Nafion solution, and 3 mL of 2-propanol under ultrasonication for 30 min. CuSus, AgNaf, and AgSus were prepared by identical preparation method but replacing Cu with Ag nanoparticles (US Research Nanomaterias Inc, ≈20 nm), and/or Nafion with Sustanion XA-9 (Dioxide Materials). The catalyst ink was spray coated on the hydrophilic (Freudenberg H23) or hydrophobic (Sigracet 22BB) carbon paper (active area: 6.25 cm^2) until the Cu or Ag mass loading was around 1 mg cm^{-2}. For the layered structure, identical catalyst ink was used and coated layer by layer with around 1 mg cm^{-2} of catalyst for each layer. To prepare the PTFE-containing catalyst layer, 37.5 mg of PTFE nanopowder (Nanoshel, 30–50 nm) was added to the Cu or Ag catalyst ink with extra addition of 2 mL of 2-propanol. For the spray coating of PTFE-containing ink, the Cu or Ag mass loading was kept to around 1 mg cm^{-2}.

Characterization

SEM images and EDS were acquired using FEI Quanta 250 FE-SEM equipped Oxfords X–Max 80 and corrected by FEI Quanta-FEG 250 SEM equipped with an Oxford Instruments Aztec EDS system. For cross-section analysis, bilayer Cu/Ag samples were vacuum-embedded into epoxy (EpoxySet 145-20005, Allied High Tech Products), with addition of 5% of iodoform, then cured overnight at room temperature. The cured samples were polished through 1 μm diamond slurry for characterization. For cross-section analysis, CuSus/AgNaf sample was embedded into iodine-epoxy and cured overnight followed by polishing with sandpaper. The static contact angles were measured by placing carbon paper-based catalysts on a flat electrode surface using a contact angle meter (MCA-4, Kyowa Interface Science Co., Ltd). One drop of 6 μL deionized (DI) water was dropped on each surface region, and the pictures were taken within 30 s. Each sample was measured at five different regions and the average was calculated.

Electrochemical measurement and flow cell set up

Electrochemical measurements were carried out on a BioLogic VSP-300 electrochemical workstation. A membrane electrode assembly (MEA)-based flow cell was used as the bicarbonate electrolyzer (Figure 1). The anode and cathode flow plates were made from stainless steel and titanium with 2.5 × 2.5 cm^2 of flow channels, respectively. A Ni foam (2.5 × 2.5 cm^2) and 40 mL of 1.0 M KOH were used as the anode and anolyte, respectively, for the oxygen evolution reaction (OER). The prepared catalyst and 40 or 120 mL of 3.0 M $KHCO_3$ were used as cathode and catholyte, respectively. Bipolar membrane (Fumatech, fumasep FBM) was used as the membrane with reverse bias mode to provide proton to the cathode side. The flow rate of both catholyte and anolyte was maintained at 50 mL min^{-1} by a peristaltic pump (Masterflex L/S), and the gaseous Ar was purged into the headspace of catholyte to carry the gaseous products out for their on-line quantification. The bicarbonate conversion performance was evaluated under the chronopotentiometry condition at the current densities from 100 to 300 mA cm^{-2}. All electrochemical tests were carried out at room temperature.

Product quantification and FE calculations

The gaseous products were analyzed by an on-line gas chromatograph (GC, SRI instrument 8610 C MG#3) equipped with HaySep D and MolSieve 5 Å columns. H_2 was detected by the thermal conductivity detector (TCD), and CO, CH_4, and C_2H_4 were detected by the flame ionization detector (FID). The rate of H_2, CO, CO_2, CH_4, and C_2H_4 generation (r, mol s^{-1}) was calculated by Equation (2):

$$r = c \times 10^{-6} \times \frac{p\dot{V} \times 10^{-6}}{RT} \tag{2}$$

where c is the concentration [ppm], $V^{\cdot}$ is the volumetric flow rate of the inlet gas (100 mL min^{-1}), p is the ambient pressure (1.013 × 10^5 Pa), R is the gas constant (8.314 J mol^{-1} K^{-1}), and T is the temperature (314.15 K). The total amount of gaseous production [mol] was calculated by integrating the plot of gaseous production rate [mol s^{-1}] vs. reaction time [s] with polynomial curve fitting. The liquid products (formate, acetate, ethanol, propanol) were quantified by proton nuclear magnetic resonance spectroscopy (^{1}H NMR, Bruker AV III 600) using the saturation method. Typically, 500 μL of sample solution was mixed with 100 μL of D_2O and dimethyl sulfoxide (DMSO) as the solvent and internal standard, respectively. After quantifying the gaseous and liquid products, the faradaic efficiency was calculated according to Eqation (3):

$$\mathrm{FE} = \frac{n \times F \times m}{Q} \tag{3}$$

where n is the number of electrons transferred for products (2 for H_2, CO, and formate, 8 for CH_4 and acetate, 12 for ethanol and ethylene, and 18 for propanol), F is the Faraday constant (96485 C mol^{-1}), m is the number of moles of gaseous or liquid products [mol], and Q is the total number of charges during the reaction time [C]. The total amount of generated *i*-CO_2 and utilization of *i*-CO_2 to C_{2+} products are calculated as follows [Eqs. (4) and (5)]:

$$\mathrm{i-CO_2} = m_{\mathrm{CO_2,GC}} + \sum n \times m_{\text{carbon containing products}} \tag{4}$$

$$\text{utilization} = \sum \frac{n \times m_{\mathrm{C_{2+}\ products}}}{\mathrm{i-CO_2}} \tag{5}$$

where $m_{CO_2,GC}$ is mole of CO_2 detected from the GC, n is the number of carbon of products (e.g., 2 for ethanol, 3 for propanol), $m_{\text{carbon containing products}}$ is mole of carbon-containing products, and $m_{C_{2+}\text{ products}}$ is mole of C_{2+} products. All the reported units used in the text and figures are mM (10^{-3} M) due to their small quantity in the CO_2 electrochemical reduction tests.

Acknowledgements

This work was supported by the IEC competitive fund (20-IEC-019) and USDA NIFA (20216702134650). We acknowledge Warren Straszheim for SEM and EDS measurement; thank Prerana Carter, Ting-Han Lee, Michael Lee, and Dr. Chris Cornelius for their help with contact angle measurement; and are grateful to fruitful discussion with Yifu Chen, Dr. Shuang Gu, Huy Nguyen, Tianlei Li, Basil Rawah, Mohammad Albloushi, Xiaopeng Liu and Yoke Qi Ho. W. Li acknowledges his Herbert L. Stiles Faculty Fellowship and NSF fund CBET-1947435. Open Access funding provided by the Iowa State University Library.

Conflict of Interest

The authors declare no conflict of interest.

Data Availability Statement

Data available on formal request of the readers.

Keywords: bicarbonate · CO_2 reduction · electrochemistry · electrode materials · multicarbon products

[1] a) D. Wakerley, S. Lamaison, J. Wicks, A. Clemens, J. Feaster, D. Corral, S. A. Jaffer, A. Sarkar, M. Fontecave, E. B. Duoss, S. Baker, E. H. Sargent, T. F. Jaramillo, C. Hahn, *Nat. Energy* **2022**, *7*, 130–143; b) X. Tan, C. Yu, Y. Ren, S. Cui, W. Li, J. Qiu, *Energy Environ. Sci.* **2021**, *14*, 765–780; c) N. Zhang, X. Zhang, Y. Kang, C. Ye, R. Jin, H. Yan, R. Lin, J. Yang, Q. Xu, Y. Wang, Q. Zhang, L. Gu, L. Liu, W. Song, J. Liu, D. Wang, Y. Li, *Angew. Chem. Int. Ed.* **2021**, *60*, 13388; d) E. Zhang, T. Wang, K. Yu, J. Liu, W. Chen, A. Li, H. Rong, R. Lin, S. Ji, X. Zheng, Y. Wang, L. Zheng, C. Chen, D. Wang, J. Zhang, Y. Li, *J. Am. Chem. Soc.* **2019**, *141*, 16569–16573.

[2] a) D. Gao, F. Scholten, B. Roldan Cuenya, *ACS Catal.* **2017**, *7*, 5112–5120; b) X. Chen, J. Chen, N. M. Alghoraibi, D. A. Henckel, R. Zhang, U. O. Nwabara, K. E. Madsen, P. J. A. Kenis, S. C. Zimmerman, A. A. Gewirth, *Nat. Catal.* **2020**, *4*, 20–27; c) J. Lee, H. Liu, Y. Chen, W. Li, *ACS Appl. Mater. Interfaces* **2022**, *14*, 14210–14217; d) M. Zhang, W. Wei, S. Zhou, D.-D. Ma, A. Cao, X.-T. Wu, Q.-L. Zhu, *Energy Environ. Sci.* **2021**, *14*, 4998–5008.

[3] a) D. W. Keith, G. Holmes, D. St. Angelo, K. Heidel, *Joule* **2018**, *2*, 1573–1594; b) M. Bui, C. S. Adjiman, A. Bardow, E. J. Anthony, A. Boston, S. Brown, P. S. Fennell, S. Fuss, A. Galindo, L. A. Hackett, J. P. Hallett, H. J. Herzog, G. Jackson, J. Kemper, S. Krevor, G. C. Maitland, M. Matuszewski, I. S. Metcalfe, C. Petit, G. Puxty, J. Reimer, D. M. Reiner, E. S. Rubin, S. A. Scott, N. Shah, B. Smit, J. P. M. Trusler, P. Webley, J. Wilcox, N. Mac Dowell, *Energy Environ. Sci.* **2018**, *11*, 1062–1176; c) O. Gutiérrez-Sánchez, B. Bohlen, N. Daems, M. Bulut, D. Pant, T. Breugelmans, *ChemElectroChem* **2022**, *9*, e202101540; d) Z. Zhang, E. W. Lees, F. Habibzadeh, D. A. Salvatore, S. Ren, G. L. Simpson, D. G. Wheeler, A. Liu, C. P. Berlinguette, *Energy Environ. Sci.* **2022**, *15*, 705–713.

[4] a) J. Sisler, S. Khan, A. H. Ip, M. W. Schreiber, S. A. Jaffer, E. R. Bobicki, C.-T. Dinh, E. H. Sargent, *ACS Energy Lett.* **2021**, *6*, 997–1002; b) A. J. Welch, E. Dunn, J. S. DuChene, H. A. Atwater, *ACS Energy Lett.* **2020**, *5*, 940–945.

[5] a) I. Sullivan, A. Goryachev, I. A. Digdaya, X. Li, H. A. Atwater, D. A. Vermaas, C. Xiang, *Nat. Catal.* **2021**, *4*, 952–958; b) E. W. Lees, J. C. Bui, D. Song, A. Z. Weber, C. P. Berlinguette, *ACS Energy Lett.* **2022**, *7*, 834–842.

[6] a) A. G. Fink, E. W. Lees, Z. Zhang, S. Ren, R. S. Delima, C. P. Berlinguette, *ChemElectroChem* **2021**, *8*, 2094–2100; b) E. W. Lees, M. Goldman, A. G. Fink, D. J. Dvorak, D. A. Salvatore, Z. Zhang, N. W. X. Loo, C. P. Berlinguette, *ACS Energy Lett.* **2020**, *5*, 2165–2173.

[7] a) T. Li, E. W. Lees, M. Goldman, D. A. Salvatore, D. M. Weekes, C. P. Berlinguette, *Joule* **2019**, *3*, 1487–1497; b) T. Li, E. W. Lees, Z. Zhang, C. P. Berlinguette, *ACS Energy Lett.* **2020**, *5*, 2624–2630.

[8] E. W. Lees, A. Liu, J. C. Bui, S. Ren, A. Z. Weber, C. P. Berlinguette, *ACS Energy Lett.* **2022**, *7*, 1712–1718.

[9] a) M. G. Kibria, J. P. Edwards, C. M. Gabardo, C. T. Dinh, A. Seifitokaldani, D. Sinton, E. H. Sargent, *Adv. Mater.* **2019**, *31*, e1807166; b) N. Han, P. Ding, L. He, Y. Li, Y. Li, *Adv. Energy Mater.* **2019**, *10*, 1902338; c) X. An, S. Li, X. Hao, Z. Xie, X. Du, Z. Wang, X. Hao, A. Abudula, G. Guan, *Renewable Sustainable Energy Rev.* **2021**, *143*, 110952; d) B. An, Z. Li, Y. Song, J. Zhang, L. Zeng, C. Wang, W. Lin, *Nat. Catal.* **2019**, *2*, 709–717; e) T. N. Nguyen, J. Guo, A. Sachindran, F. Li, A. Seifitokaldani, C.-T. Dinh, *J. Mater. Chem. A* **2021**, *9*, 12474–12494; f) H. Chen, Z. Wang, X. Wei, S. Liu, P. Guo, P. Han, H. Wang, J. Zhang, X. Lu, B. Wei, *Appl. Surf. Sci.* **2021**, *544*, 148965.

[10] a) A. Vasileff, C. Xu, Y. Jiao, Y. Zheng, S.-Z. Qiao, *Chem* **2018**, *4*, 1809–1831; b) C. G. Morales-Guio, E. R. Cave, S. A. Nitopi, J. T. Feaster, L. Wang, K. P. Kuhl, A. Jackson, N. C. Johnson, D. N. Abram, T. Hatsukade, *Nat. Catal.* **2018**, *1*, 764–771; c) L. Wang, H. Peng, S. Lamaison, Z. Qi, D. M. Koshy, M. B. Stevens, D. Wakerley, J. A. Z. Zeledón, L. A. King, L. Zhou, *Chem Catal.* **2021**, *1*, 663–680; d) T. Zhang, J. C. Bui, Z. Li, A. T. Bell, A. Z. Weber, J. Wu, *Nat. Catal.* **2022**, *5*, 202–211; e) C. Kim, J. C. Bui, X. Luo, J. K. Cooper, A. Kusoglu, A. Z. Weber, A. T. Bell, *Nat. Energy* **2021**, *6*, 1026–1034.

[11] Y. C. Li, G. Lee, T. Yuan, Y. Wang, D.-H. Nam, Z. Wang, F. P. García de Arquer, Y. Lum, C.-T. Dinh, O. Voznyy, E. H. Sargent, *ACS Energy Lett.* **2019**, *4*, 1427–1431.

[12] a) C.-T. Dinh, T. Burdyny, G. Kibria Md, A. Seifitokaldani, M. Gabardo Christine, F. P. García de Arquer, A. Kiani, P. Edwards Jonathan, P. De Luna, S. Bushuyev Oleksandr, C. Zou, R. Quintero-Bermudez, Y. Pang, D. Sinton, H. Sargent Edward, *Science* **2018**, *360*, 783–787; b) C. Choi, S. Kwon, T. Cheng, M. Xu, P. Tieu, C. Lee, J. Cai, H. M. Lee, X. Pan, X. Duan, W. A. Goddard, Y. Huang, *Nat. Catal.* **2020**, *3*, 804–812; c) F. P. García de Arquer, C.-T. Dinh, A. Ozden, J. Wicks, C. McCallum, R. Kirmani Ahmad, D.-H. Nam, C. Gabardo, A. Seifitokaldani, X. Wang, C. Li Yuguang, F. Li, J. Edwards, J. Richter Lee, J. Thorpe Steven, D. Sinton, H. Sargent Edward, *Science* **2020**, *367*, 661–666.

[13] L. Fan, C.-Y. Liu, P. Zhu, C. Xia, X. Zhang, Z.-Y. Wu, Y. Lu, T. P. Senftle, H. Wang, *Joule* **2022**, *6*, 205–220.

[14] a) A. J. Garza, A. T. Bell, M. Head-Gordon, *ACS Catal.* **2018**, *8*, 1490–1499; b) J. Li, Z. Wang, C. McCallum, Y. Xu, F. Li, Y. Wang, C. M. Gabardo, C.-T. Dinh, T.-T. Zhuang, L. Wang, J. Y. Howe, Y. Ren, E. H. Sargent, D. Sinton, *Nat. Catal.* **2019**, *2*, 1124–1131.

Manuscript received: July 14, 2022
Revised manuscript received: September 12, 2022
Accepted manuscript online: September 18, 2022
Version of record online: October 10, 2022